International Journal of Heat and Mass Transfer 51 (2008) 3259–3266

Contents lists available at ScienceDirect

International Journal of Heat and Mass Transfer

journal homepage: www.elsevier.com/locate/ijhmt

Deteriorated turbulent heat transfer (DTHT) of gas up-flow in a circular tube: Experimental data

J.I. Lee [a], P. Hejzlar [a,*], P. Saha [a], P. Stahle [a], M.S. Kazimi [a], D.M. McEligot [b]

[a] Department of Nuclear Science and Engineering, Massachusetts Institute Technology, 77 Massachusetts Avenue, Rm 24-215 A, Cambridge, MA 02139, USA
[b] Idaho National Laboratory, Idaho Falls, ID 83415-3885, USA

ARTICLE INFO

Article history:
Received 6 July 2007
Received in revised form 7 March 2008
Available online 20 May 2008

Keywords:
Deteriorated turbulent heat transfer
Buoyancy
Acceleration

ABSTRACT

The major focus of this paper is to present experimental data, collected for three gases – nitrogen, helium, and carbon dioxide, at the deteriorated turbulent heat transfer (DTHT) regime in gas up-flow with near uniform heat flux. The data were collected for a range of (1) inlet Reynolds number from 1800 to 42,700, (2) inlet buoyancy number Bo^* up to $1 \times 10^{-5}$and (3) inlet acceleration parameter K_v up to 5×10^{-6}. Based on the new experimental data, the traditional thresholds for the DTHT regimes are updated, and a new heat transfer regime map is proposed and compared to the existing experimental data.

1. Introduction

The characteristics of convective heat transfer start to depart from the forced convection theory and the traditional correlations when the applied heat flux is high enough to affect the flow pattern. High heat flux usually induces a change in the transport properties of a fluid, such as the viscosity and thermal conductivity, and also lowers the fluid density. Multiplication of the forced convection correlation by the wall-to-bulk temperature ratio with an appropriate power is typically sufficient to account for the variation of transport properties due to heating. In contrast, a stream-wise density variation, which can be significant in gas flow, can result in more complex phenomena.

The first major phenomenon is a buoyancy effect. The buoyancy effect on the flow varies with the flow orientation and heating direction (from wall to fluid or from fluid to wall). This study will address only upward heated flow (from wall to fluid) since this is the situation in a gas cooled fast reactor cooling channel, which was the main focus of this research. More details of the gas cooled fast reactor system can be found in Refs. [1,2].

The buoyancy effect can alter the heat transfer characteristics of both laminar and turbulent flows. In laminar flow, the buoyancy force produces a steeper velocity gradient near the heated wall than in the normal forced flow, resulting in more pronounced heat convection near the wall. Typically such a situation where a strong buoyancy force is acting on the forced convection flow is called the "mixed convection" regime.

In contrast to laminar flow, turbulent flow shows more complicated behavior with respect to the buoyancy effect. The buoyancy force accelerates the flow near the wall more than the bulk flow, thus altering the normal turbulent velocity profile. The shear stress on the fluid elements near the boundary between the wall and the turbulent core decreases due to the velocity profile modification, and reduction of turbulence generation follows reduction of the shear stress. Therefore, the turbulent heat transport is "deteriorated" [3]. The resulting governing non-dimensional number that was developed in Ref. [3] is called the buoyancy parameter, Bo^*, and is defined in Eq. (1). All non-dimensional numbers in Eq. (1) are evaluated at the local bulk temperature.

$$Bo^* = \frac{Gr_q}{Re^{3.425}\,Pr^{0.8}} \tag{1}$$

An acceleration effect is the second phenomenon induced by a fluid density change. As the fluid bulk temperature along the heated channel increases, the gas density is reduced. The fluid density decrease is accompanied by bulk velocity rise to satisfy continuity of mass, resulting in the stream-wise acceleration of the flow. The stream-wise flow acceleration, which corresponds to a favorable pressure gradient, decreases the turbulence of the flow [4]. The turbulent flow behaves more like a laminar flow (sometimes the term "laminarization" is used) and the turbulent heat transfer capability can decrease drastically.

The flow acceleration was well studied in converging channels, where the mean velocity of the flow is forced to increase due to the decrease in the flow area [4]. A strongly heated flow exhibits behavior similar to the converging channels. The condition for measuring the importance of this effect is given in terms of the acceleration parameter in the converging channel case (the first

* Corresponding author. Tel.: +1 617 253 4231; fax: +1 617 258 8863.
E-mail address: hejzlar@mit.edu (P. Hejzlar).

0017-9310/$ - see front matter © 2008 Elsevier Ltd. All rights reserved.
doi:10.1016/j.ijheatmasstransfer.2008.03.021

Nomenclature

Bo^*	buoyancy parameter = $Gr_q/Re^{3.425}\ Pr^{0.8}$
c_p	specific heat at constant pressure (J/kg K)
D	pipe diameter (m)
G	mass flux (kg/m^2 s)
g	gravitational acceleration (m/s^2)
Gr_q	Grashof number based on heat flux = $g\beta q''_w D^4/k\nu^2$
H	enthalpy (J/kg)
h	heat transfer coefficient (W/m^2 K)
K_ν	acceleration parameter = $\nu/U_b^2(dU_b/dx) \approx 4q^+/Re$
k	thermal conductivity (W/m K)
L	distance from the inlet (m)
$\dot{m}$	mass flow rate (kg/s)
Nu	Nusselt number = hD/k
P	system pressure (MPa)
Pr	Prandtl number = ν/α
q^+	non-dimensional heat flux = $q''_w/GH_b \approx q''_w/Gc_pT_b \approx \beta q''_w/Gc_p$
q''	heat flux (W/m^2)
Re	Reynolds number = U_bD/ν
T	temperature (K)
U	velocity (m/s)
x	axial direction and distance (m)

Greek symbols

α	thermal diffusivity = $k/\rho c_p$ (m^2/s)
β	thermal expansion coefficient $-1/\rho(\partial\rho/\partial T)_p$ (K^{-1})
μ	dynamic viscosity (kg/m s)
ν	kinematic viscosity (m^2/s)
ρ	density (kg/m^3)

Subscripts

b	bulk
F	forced convection
in	inlet
th	threshold
w	wall

part of Eq. (2)). According to Ref. [5], the acceleration parameter can be approximated by the ratio of non-dimensional heat flux over the Reynolds number when it is applied to strongly heated flow cases (the second part of Eq. (2)). The approximation was obtained by applying an energy balance and continuity equation with perfect gas and constant cross-section assumptions to the original definition of K_ν. All the non-dimensional numbers in Eq. (2) are evaluated at the bulk temperature.

$$K_\nu = \frac{\nu}{U_b^2}\frac{dU_b}{dx} \approx \frac{4q^+}{Re} \tag{2}$$

The threshold values for the buoyancy and acceleration effects to cause a transition from the normal turbulent heat transfer to the deteriorated turbulent heat transfer (DTHT) regime have been reported to be $Bo^* \sim 6 \times 10^{-7}$ and $K_\nu \sim 3 \times 10^{-6}$, respectively [6]. The regime, where normal turbulent convective heat transfer is hindered by either of these two phenomena, thereby reducing the fluid heat transfer capability, is called the DTHT regime. Even though the onset of this regime due to the acceleration or buoyancy effect is reasonably well defined, the heat transfer coefficient values and correlations in these regimes are still under discussion. Detailed reviews of the literature on mixed convection and transition heat transfer regimes and the heat transfer correlations, are provided in Refs. [7,8].

Conditions for DTHT can be encountered in a nuclear system during an anticipated transient. In particular, the Generation IV gas-cooled fast reactor (GFR), which is under development in the US, France, and Japan, has a possibility to operate in the DTHT regime during post-loss-of-coolant accident (LOCA) conditions (see Refs. [2,9,11]). For example, a block-core configuration [1], which is one of the GFR design candidates, has the potential to operate in the DTHT regime or in the transition between the DTHT and normal forced or laminar convection regimes during LOCA conditions [2]. As discussed in Ref. [10,11], the dependence of gas thermophysical properties on temperature is very different from that of supercritical fluid and liquid water. Therefore, even though a large body of experimental data exists for supercritical fluid and liquid water, it is not appropriate to utilize their data for predicting gas heat transfer before it is thoroughly examined. Consequently, a need emerged to expand the gas heat transfer experimental database to aid the general understanding of the DTHT regimes and the important underlying physical phenomena to be able to develop reliable correlations for the design of the GFR and comparable systems.

This paper will present data for three different gases, namely: nitrogen, helium and carbon dioxide, and finally show a newly proposed heat transfer regime map for the gas heated upward flow in a circular channel. Since the experimental apparatus is well described in Ref. [10], the same is not presented in this paper, except for the statement that the heated test section has an inner diameter of 15.7 mm and a length of 2 m.

2. Experimental data

The data presented in this paper will be given in non-dimensional forms, as obtained through the data reduction process, except for a few cases where the temperature profile can provide some physical insight. All non-dimensional numbers presented in this section are evaluated at the local bulk temperature, unless specifically indicated otherwise. Table 1 briefly summarizes the operating conditions for all experimental runs. It should be noted that all three gases were operated far from their critical points.

Within this work, the heat transfer regimes are defined as follows:

- The laminar regime and mixed convection laminar regime are for inlet Reynolds numbers smaller than 2300.
- The transition regime is at an inlet Reynolds number above 2300 but the outlet Reynolds number is below 2300.
- The turbulent regime is for both inlet and outlet Reynolds numbers above 2300.
- The DTHT regime is for both inlet and outlet Reynolds numbers above 2300 and for a reduction in the heat transfer coefficient larger than 20%. Since the forced convection correlation uncertainties are within ±20% [14], any heat transfer rate reduced by more than 20% is considered to be in the DTHT.

The operating flow regimes were the (1) mixed convection laminar, (2) transition from laminar to turbulent, (3) normal turbulent, (4) buoyancy induced DTHT and (5) acceleration induced DTHT regimes, as can be seen from comparing Table 1 to the threshold values for the DTHT in Ref. [6] ($Bo^* \sim 6 \times 10^{-7}$ and $K_\nu \sim 3 \times 10^{-6}$).

Table 1
Summary of experimental parameters for all runs

	All	N_2	He	CO_2
Total number of runs	58 (N_2, He, CO_2)	20	15	23
Run numbers	1–58	1–20	21–35	36–58
Operating pressure range (MPa)	0.13–0.67	0.13–0.59	0.17–0.40	0.13–0.67
Operating power range (W)	200–2690	291–1989	200–2630	720–2690
Operating volumetric flow rate range (m^3/s)	$0.19–2.88 \times 10^{-3}$	$0.24–2.88 \times 10^{-3}$	$1.17–2.88 \times 10^{-3}$	$0.19–2.83 \times 10^{-3}$
Inlet temperature (K)	300–305	~302	~304	~303
Inlet Reynolds number range	1800–42,700	5300–23,600	1800–4500	12,000–42,700
Inlet q^+ range	0.0003–0.0039	0.0003–0.0036	0.0003–0.0039	0.0006–0.0022
Inlet Bo^* range	$3 \times 10^{-9}–1 \times 10^{-5}$	$3 \times 10^{-9}–6 \times 10^{-6}$	$7 \times 10^{-9}–4 \times 10^{-7}$	$1 \times 10^{-8}–1 \times 10^{-5}$
Inlet K_v range	$6 \times 10^{-8}–5 \times 10^{-6}$	$6 \times 10^{-8}–3 \times 10^{-6}$	$4 \times 10^{-7}–5 \times 10^{-6}$	$8 \times 10^{-8}–8.5 \times 10^{-7}$

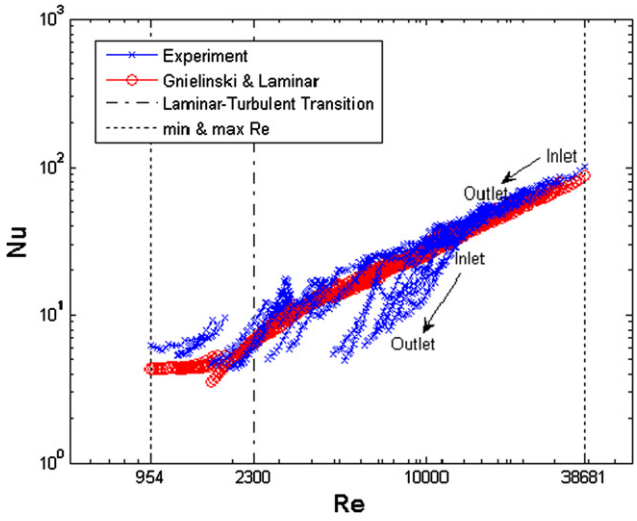

Fig. 1. Summary of all data in *Nu*–*Re* plot.

Fig. 1 depicts the local Nusselt number versus Reynolds number along with the laminar correlation (Eq. (3)) [4] and the Gnielinski correlation (Eq. (4)) [14] predictions. Even though 20 thermocouples were attached to the heated section, only 16 data points per case are shown in Fig. 1. This limitation is because the first and last two points have relatively larger uncertainties due to axial heat loss by conduction to the power taps located at each end of the heated section [12,13]:

$$Nu_{\text{Laminar}} = \left(\frac{1}{Nu_\infty} - \frac{1}{2}\sum_{m=1}^{\infty}\frac{\exp(-\gamma_m^2 x^+)}{A_m\gamma_m^4}\right)^{-1} \approx \left(\frac{1}{Nu_\infty} - \frac{1}{2}\sum_{m=1}^{10}\frac{\exp(-\gamma_m^2 x^+)}{A_m\gamma_m^4}\right)^{-1} \quad (3)$$

where $Nu_\infty = 4.364$, $x^+ = \frac{2L/D}{Re\,Pr}$, $\gamma_m = 4m + \frac{4}{3}$, $A_m = 0.4165\gamma_m^{-7/3}$

$$Nu_{\text{Gnielinski}} = \frac{(f/8)(Re - 1000)\,Pr}{1 + 12.7\sqrt{f/8}(Pr^{2/3} - 1)}\left(\frac{T_w}{T_b}\right)^{-0.45}\left(1 + \left(\frac{L}{D}\right)^{-\frac{2}{3}}\right) \quad (4)$$

where $f = (1.82\log_{10}Re - 1.64)^{-2}$.

For the laminar correlation, the sum of the series was stopped at 10 terms, even though theoretical analysis calls for infinite summation. The value of 10 was selected since the total value changes by <1% when adding more terms to the summation, a result which is considered acceptable with respect to correlation uncertainties. It is also important to note that the Gnielinski correlation range stops at a local Reynolds number of 2300; but irrespective of the value of local Reynolds number, the Gnielinski correlation was still used to predict the Nusselt number if the inlet Reynolds number was higher than 2300. This scheme was applied to obtain continuous axial heat transfer coefficients inside the heated channel. It is noted that, due to the entrance effect term in the Gnielinski correlation, multiple Nusselt numbers can exist for the same local Reynolds number. Thus, the Gnielinski correlation in Fig. 1 is not a single curve. In order to differentiate cases from each other, data points for the same operating conditions are connected with a line.

Before starting the discussion of which effect is responsible for inducing the DTHT, the values for each threshold need to be revised to compare both effects reasonably. The acceleration parameter threshold identifies when the turbulent flow becomes fully laminarized and the heat transfer coefficient decreases from the turbulent flow value to the laminar flow value [6]. The minimum reduction for the fully acceleration driven DTHT can be calculated for this case by taking the ratio of the laminar Nusselt number for constant wall heat flux for fully established conditions ($Nu = 4.364$) to the turbulent Nusselt number at the Reynolds number of 2300 ($Nu = 7.211$ at $Pr = 0.7$ from Gnielinski correlation), which yields 4.364/7.211 = 0.605. Therefore, the minimum reduction for which the acceleration parameter exceeded the threshold, would have been approximately 40%.

In contrast, the buoyancy parameter threshold is typically set at a point where the measured Nusselt number is reduced from the forced convection turbulent flow Nusselt number by 5% ($Bo^* \approx 6 \times 10^{-7}$) [6,14]. The buoyancy and acceleration effects are not treated consistently in the literature as acceleration is only considered to have significant impact at 40% and higher heat transfer reductions while a buoyancy driven reduction of only 5% is considered significant. Moreover, one needs to keep in mind that the uncertainty of even the well known forced convection correlations can be about 20% [14]. Therefore, we suggest an increase of the threshold at which the buoyancy driven laminarization is considered to have a significant impact on heat transfer so that the effect is on par with the acceleration effect and is more consistent with uncertainties of forced convection correlations.

To have a comparable buoyancy parameter threshold to the acceleration threshold, the buoyancy threshold is redefined as the buoyancy number that gives the same fractional reduction of the Nusselt number compared to the acceleration threshold. This value can be estimated using Jackson's heat transfer correlation [15]. Since we adopted the buoyancy parameter developed by Hall and Jackson and the heat transfer correlation presented in Ref. [15] is based on their studies, Eq. (5) is chosen to maintain the consistency.

$$\frac{Nu_{\text{Jackson}}}{Nu_F} = \left(1 - \frac{8 \times 10^4\, Bo^*}{(Nu_{\text{Jackson}}/Nu_F)^2}\right)^{0.46} \quad (5)$$

A 40% reduction in the Nusselt number can be obtained by setting the ratio (Nu_{Jackson}/Nu_F) to 0.6 in Eq. (5) and then solving for the equivalent buoyancy parameter threshold which would be $Bo^* \approx 3 \times 10^{-6}$. Therefore, $Bo^* \approx 3 \times 10^{-6}$ will be taken as a buoyancy DTHT threshold and used for comparing the relative strength

of the buoyancy effect versus the acceleration effect. $Bo^* \approx 3 \times 10^{-6}$ will be denoted as "Equivalent" threshold and $Bo^* \approx 6 \times 10^{-7}$ will be denoted as "Ref." threshold in this paper.

Figs. 2 and 3 show the ratios of measured over predicted Nusselt numbers using the Gnielinski correlation versus the buoyancy and acceleration parameters, respectively. Both thresholds (Ref. [6] threshold and the equivalent threshold) for the buoyancy induced DTHT are shown in Fig. 2 while Fig. 3 shows the threshold of the acceleration induced DTHT from Ref. [6]. The maximum reduction in the local heat transfer coefficient compared to the Gnielinski correlation is 76% (Run 20). Also, it is noted that neither the buoyancy nor acceleration parameters, based on local bulk conditions, successfully correlates the data in the regions demarcated by the thresholds.

Table 1 shows that the nitrogen runs (1–20) are all in the normal turbulent flow heat transfer regime and some high heat flux runs are in the DTHT regimes, since the buoyancy and acceleration parameters were above or near the threshold indicated by Ref. [6]. Runs 4, 6, and 17–20 are the runs that operated in the DTHT regime, while the rest of the nitrogen runs were in the normal turbulent flow regime.

Figs. 4 and 5 plot the axial temperature profiles of the two DTHT runs (6 and 17) of interest together with the normal forced turbulent heat transfer runs (7 and 16). These runs were chosen so that the operating pressure would be nearly the same between Runs 6, 7 and Runs 17, 16.

In Fig. 4, the dotted line, which is indicated as T_{wG} in the legend, is the predicted wall temperature using the Gnielinski correlation for the turbulent heat transfer. The measured wall temperature of Run 6 is significantly higher than the predicted wall temperature (maximum difference is 98 °C). If we compare measured and predicted wall temperatures for Run 6 to those of Run 7, Run 6 was operating in the DTHT regime exhibiting significant reduction in the heat transfer coefficient. Run 6 was operated at $K_{v_{in}} \approx 3.0 \times 10^{-6}$ and $Bo^*_{in} \approx 8.1 \times 10^{-7}$. Considering the previous discussion on determination of the equivalent buoyancy threshold ($Bo^* \approx 3.0 \times 10^{-6}$), the deterioration of heat transfer apparently occurred due to the significant acceleration effect rather than the buoyancy effect.

In Fig. 5, again the dotted line (T_{wG}) is the predicted wall temperature using the Gnielinski correlation. The measured wall temperature for Run 17 is significantly higher than the predicted wall temperature (maximum difference is 199 °C). Such a large difference between measured and predicted wall temperatures of Run 17 in comparison to Run 16 is a consequence of significant reduction in the heat transfer coefficient of Run 17. Thus, Run 17

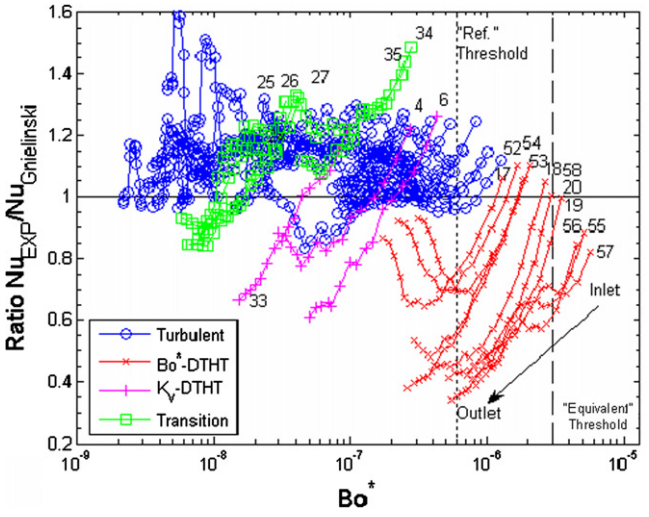

Fig. 2. Summary of data in *Nu* ratio–Bo^* plot.

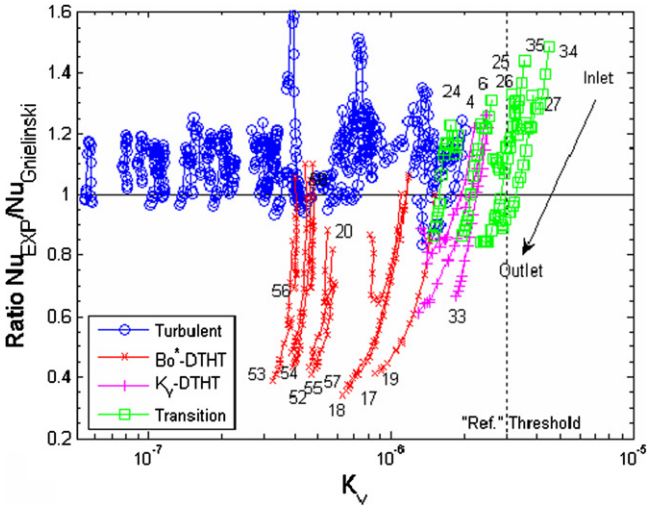

Fig. 3. Summary of data in *Nu* ratio–K_v plot.

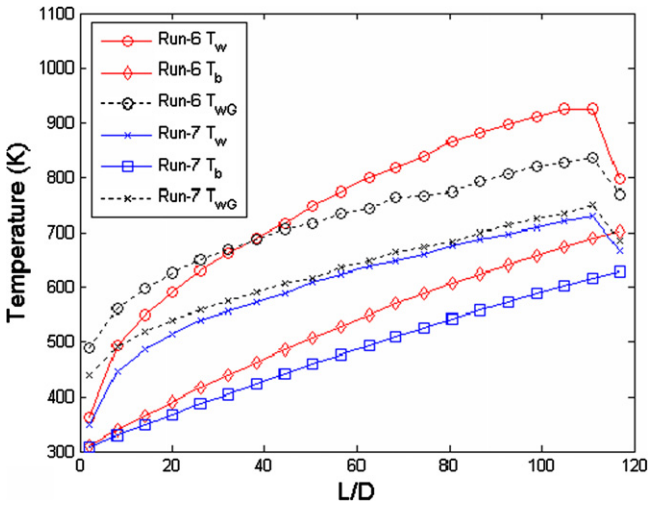

Fig. 4. Measured and predicted wall temperature profiles from nitrogen Runs 6 and 7.

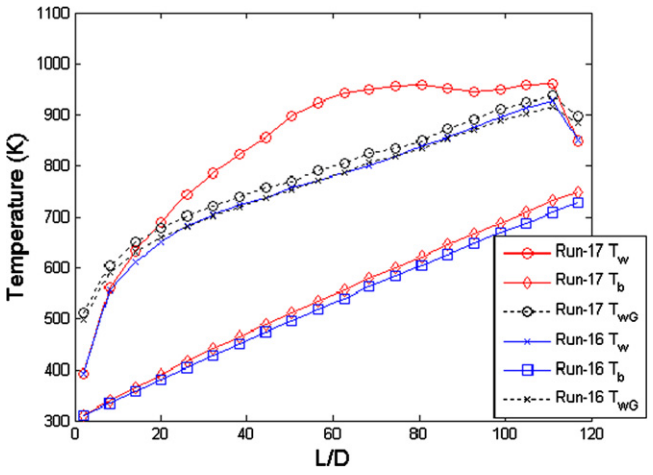

Fig. 5. Measured and predicted wall temperature profiles from nitrogen Runs 16 and 17.

was operating in the DTHT regime. Since Run 17 had a large Bo^* number, $Bo^*_{in} \approx 2.1 \times 10^{-6}$ (~70% of the equivalent threshold $Bo^* \approx 3.0 \times 10^{-6}$) and $K_{v_{in}} \approx 1.3 \times 10^{-6}$ (~40% of the threshold $K_v \approx 3.0 \times 10^{-6}$), this deterioration is likely caused by the buoyancy effect.

An interesting observation that can be made from Figs. 4 and 5 is that the wall temperature profiles between the acceleration induced DTHT and the buoyancy induced DTHT differ from each other in these cases. The acceleration effect driven DTHT gradually laminarizes the turbulent flow downstream until the heat transfer coefficient reaches the value of laminar heat transfer coefficient at the end of the test section, while the buoyancy effect driven DTHT exhibits maximum deterioration in the middle of the channel. Since the buoyancy parameter decreases along the channel for the heated gas flow due to the gas thermo-physical properties variation, the buoyancy effect also decreases along the channel. After a certain reduction of the buoyancy force occurs, the flow regains its turbulent intensity and approaches the normal turbulent flow. To describe this phenomenon occurring in a buoyancy driven mixed convection flow in a heated channel, we adopted the term "re-turbulization" of the laminarized flow. This phenomenon will be addressed in more detail when the carbon dioxide data are discussed.

Table 1 shows that the helium runs (21–35) have the potential for covering the laminar, mixed convection laminar, transition between laminar and turbulent, turbulent, and acceleration driven DTHT regimes as we defined them. The actual helium experiments operated in the mixed convection laminar, transition, turbulent, and DTHT regimes, as can be seen in Figs. 2 and 3. Runs 28–30 were in the mixed convection laminar flow regime, Runs 25–27 and 34–35 were in the transition regime, Runs 21–24 and 31–32 were in the turbulent regime and finally Run 33 was in the DTHT regime.

It is interesting to note that even though several runs in the transition flow category (i.e., Runs 25–27 and 34–35) have a stronger acceleration effect than the DTHT runs, their heat transfer coefficient is not reduced more than 20% relative to the Gnielinski correlation. This may be a consequence of "turbulization" of laminar flow due to strong heating. It has been documented that the laminar to turbulent transition can occur at a local Reynolds number below 2300 in the heated flow where heating causes instability of the stable flow [8]. Therefore, there could be two competing effects – the buoyancy force driven "turbulization" of laminar flow and the acceleration, which induces the "laminarization" of the turbulent flow. If the turbulization process becomes stronger than the laminarization effect, the convection heat transfer would increase compared to the predicted values. As the turbulence is generated from the velocity gradient, a steeper gradient between the wall and the peaks of the double-hump velocity profile typical for highly heated flow can create a strong flow instability, enough to maintain the turbulence in spite of the strong stream-wise acceleration effect. The enhancement of the heat transfer coefficient in the transition regime, when compared to the Gnielinski correlation, follows the increase of the buoyancy parameter and supports this hypothesis, which can be observed in Fig. 2 (Runs 25, 26, 27, 34 and 35).

Figs. 2 and 3 also show that the measured value of the helium turbulent forced heat transfer coefficient is the highest above the Gnielinski correlation prediction when both the buoyancy effect and the acceleration effect are small. This was unexpected and more data would be needed to check the reproducibility of this observation and identify what physical phenomena are behind this unexpected increase.

The carbon dioxide runs (36–58) operated in the forced turbulent and buoyancy induced DTHT regimes, as shown in Table 1. Runs 52–58 operated in the DTHT regime and the rest of the runs operated in the normal turbulent forced convection regime. The temperature profile of the non-re-turbulizing flow is shown in Fig. 6. Runs 50 (inlet $Bo^* = 1.77 \times 10^{-6}$) and 57 (inlet $Bo^* = 1.11 \times 10^{-5}$) are compared to illustrate the wall temperature for non-re-turbulizing flow. Comparing Figs. 5 to Figs. 6, one can conclude that as the inlet buoyancy parameter increases the wall temperature peak moves toward the downstream end of the channel in these cases.

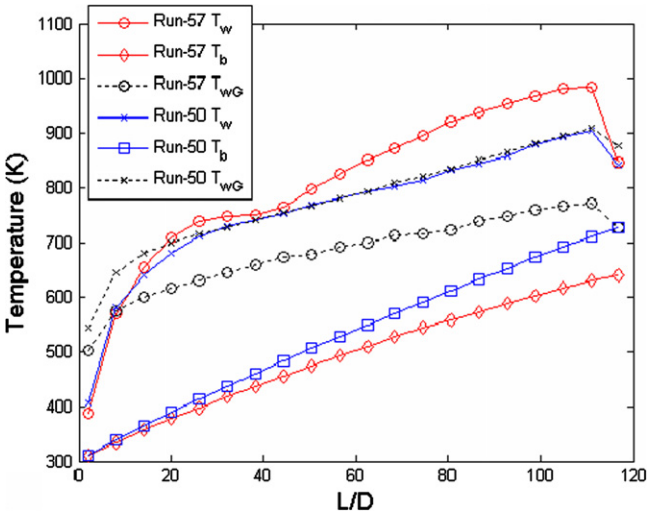

Fig. 6. Temperature profiles of non-re-turbulizing flow (carbon dioxide Runs 50 and 57).

The nitrogen data and carbon dioxide data indicate that the buoyancy induced DTHT regime can exhibit two temperature profile trends and may need to be further divided into "re-turbulizing" and "non-re-turbulizing" regimes. If we further divide the buoyancy induced DTHT into two sub-regimes, i.e. re-turbulizing flow and non-re-turbulizing flow, the boundary between the two can be decided from Fig. 7. Fig. 7 shows the inlet buoyancy number of DTHT runs with the location of maximum heat transfer reduction. The value $Bo^*_{in} = 3.5 \times 10^{-6}$ is identified from Fig. 7 as an approximate boundary between the re-turbulizing flow and non-re-turbulizing flow. The re-turbulized runs are defined as those where the maximum reduction occurred near the middle of the test section ($L/D \approx 60$), and the non-re-turbulized flows are defined as those where the maximum reduction occurred near the outlet of the test section ($L/D \approx 110$). The apparent threshold of the

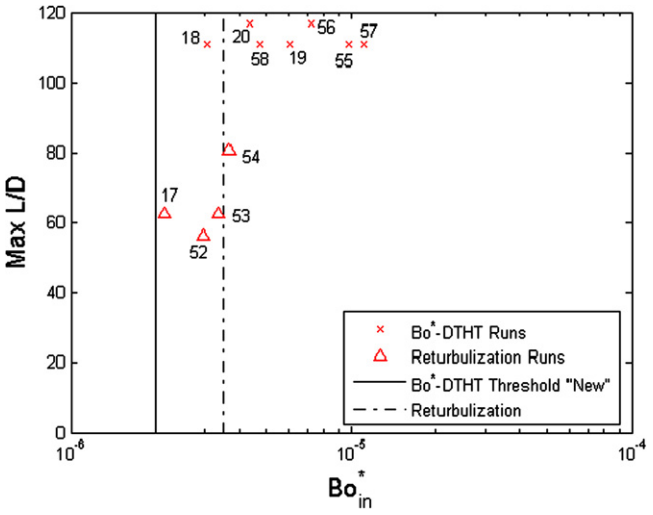

Fig. 7. Locations of maximum reductions versus inlet buoyancy parameters (shows both nitrogen and carbon dioxide runs together).

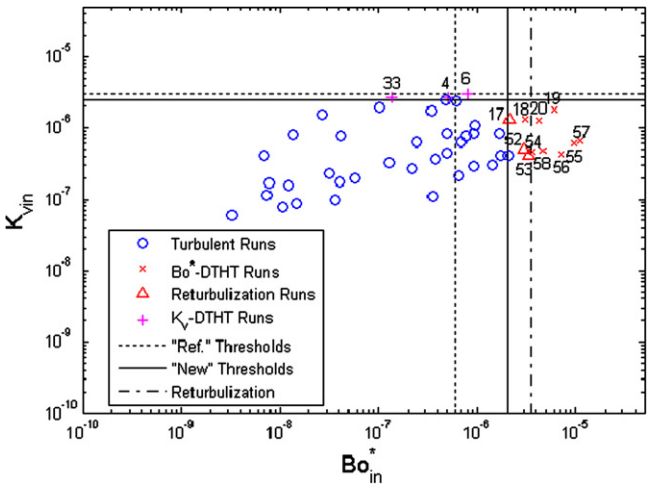

Fig. 8. Inlet acceleration parameter versus inlet buoyancy parameter for three gases with minimum channel Reynolds numbers (outlet) larger than 2300.

buoyancy induced DTHT regime also was shifted from $Bo^*_{in} = 3.0 \times 10^{-6}$ ("Equivalent" threshold) to $Bo^*_{in} = 2.0 \times 10^{-6}$ ("New" threshold) in Fig. 7, to have a better correlation of these data with the threshold value.

Fig. 8 is a presentation of normal turbulent and DTHT runs relative to their inlet buoyancy numbers and the acceleration numbers. The figure also shows the original threshold value indicated in Ref. [6] and the new thresholds identified from the data obtained at this experimental facility. Figs. 2 and 3 show that using the local buoyancy number and local acceleration number can be ambiguous for determining the dominant physical effect, while Fig. 8 implies that *inlet values can successfully demarcate buoyancy driven and acceleration driven DTHT* for channels with uniform heat flux. Therefore, the inlet values are chosen to show each effect. The newly acquired data indicate that the threshold of acceleration driven DTHT should also be shifted from $K_{v_{in}} = 3.0 \times 10^{-6}$ ("Ref.") to $K_{v_{in}} = 2.5 \times 10^{-6}$("New") in order to better reflect the gas heat transfer data.

The maximum measurement uncertainties were within 10%, other than for the low Reynolds number runs. The low Reynolds number runs, which were performed with helium, had higher uncertainties (up to 25%). The reason for the helium low Reynolds number run having higher uncertainties is due to taking the uncertainties in the gas thermo-physical properties into consideration. In other words, the uncertainties of measurement devices were the major source of the total uncertainty most of time, but some low Reynolds number runs were also appreciably affected by uncertainties in the gas properties. In short, most nitrogen and carbon dioxide runs had low uncertainties (below 10%) and are thus reliable data. The helium data are more difficult to obtain with high accuracy due to a small wall-to-bulk temperature differences (due to the high helium conductivity) and small flow rates. Nevertheless, they had relatively low uncertainties; below 15% for most of the runs and only one run reaching 25%.

3. Proposed gas heat transfer map for heated gas up-flow through circular channels

The heat transfer regime map has been under continuous development by various investigators since the work of Metais and Eckert [16]. In this section, a heat transfer regime map will be developed with a new non-dimensional number and thresholds for transition among the heat transfer regimes based on the data obtained in these experiments. The basic parameters that will be used here are the non-dimensional heat flux q^+ and the Reynolds number.

The thresholds for the acceleration driven DTHT and the buoyancy driven DTHT were changed in the previous section ("New" thresholds), and these thresholds can be translated into relationships between q^+ and Re using Eqs. (6) and (7).

$$K_{v_{th}} = \frac{4q^+}{Re} \approx 2.5 \times 10^{-6} \Rightarrow Re = 1.6 \times 10^6 q^+ \tag{6}$$

$$Bo^*_{th} = \frac{Gr_q}{Re^{3.425} Pr^{0.8}} \approx 2 \times 10^{-6} \Rightarrow Re = \left(5 \times 10^5 \left(\frac{gD^3}{\alpha^{0.2}\nu^{1.8}}\right) q^+\right)^{0.4124} \tag{7}$$

since $Gr_q = \frac{g\beta q''_w D^4}{k\nu^2} = \frac{\beta q''_w}{Gc_p}\frac{GD}{\mu}\frac{\alpha}{\nu}\frac{\rho c_p}{k}\frac{gD^3}{\alpha} \approx \frac{q^+ Re}{Pr}\frac{gD^3}{\alpha^2}$

It should be noted that there are different versions of the non-dimensional heat flux q^+ such as $q''_w/GH_b, q''_w/Gc_pT_b$, and $\beta q''_w/Gc_p$. With an ideal gas assumption, these definitions become the same but for a real gas, such as nitrogen or carbon dioxide, different definitions can result in differences in calculated values. In the data reduction process and the correlation development process in our companion paper [7], the first definition was always used, since it is directly the ratio of the wall heat flux to the flow enthalpy flux, which has a physical meaning while the others are approximations to the first definition. Also, when performing numerical calculations, the first definition may avoid an integrating procedure, thereby simplifying the calculations, since the bulk temperature is generally deduced from the local bulk enthalpy.

The buoyancy effect threshold also includes a variable other than q^+ and Re: which is an another non-dimensional number $(gD^3/\alpha^{0.2}\nu^{1.8})$. This parameter is a function of temperature and pressure, since the thermal diffusivity and the kinematic viscosity are gas properties which vary with inlet temperature and operating pressure. A rough estimate of the non-dimensional number (Eq. (8)) can be derived, because gas properties can be generally approximated by $\rho \sim PT^{-1}$, $k \sim T^{0.8}$, $c_p \sim T^{0.1}$, and $\mu \sim T^{0.7}$.

$$\left(\frac{gD^3}{\alpha^{0.2}\nu^{1.8}}\right) = C\left(\frac{\rho c_p}{k}\right)^{0.2}\left(\frac{\rho}{\mu}\right)^{1.8} \sim CP^2T^{-3.4}, \text{ where } C = gD^3 \tag{8}$$

In addition, when the value of $(gD^3/\alpha^{0.2}\nu^{1.8})$ is less than 2.47×10^5, the acceleration tends to be the major physical effect that induces DTHT for any given q^+ and Re combinations, because the acceleration parameter exceeds the threshold earlier than the buoyancy parameter does. Thus, when the diameter is small the acceleration effect is the more pronounced mechanism for reducing the turbulent heat transfer, as this parameter is proportional to the cube of the diameter.

A tentative heat transfer map was developed and it is shown in Fig. 9. The "PGN" (property group number) in the figure denotes the non-dimensional number $(gD^3/\alpha^{0.2}\nu^{1.8})$. Two different values are chosen to show how the buoyancy threshold changes with the variation of $(gD^3/\alpha^{0.2}\nu^{1.8})$. Within the presented experimental data, $(gD^3/\alpha^{0.2}\nu^{1.8})$ at the inlet varies from 6000 to 2×10^7 depending on the operating pressure and the gas. However, the temperature and diameter influences were not examined in the experiment, since the inlet temperature was kept nearly constant and the diameter was fixed. The proposed heat transfer regime map should be used with the inlet conditions, since all the thresholds employed are defined with the inlet buoyancy number and the inlet acceleration number.

If we compare Fig. 9 to the map by Metais and Eckert [16], some significant differences between these two maps emerge. First of all, their map covers only the buoyancy effect of the turbulent heat transfer regime while the proposed map (Fig. 9) covers the acceleration effect as well. This difference occurs because the Grashof (Gr) number, which is the major variable on the abscissa of the previous map [16], cannot represent the acceleration effect directly. To cover the acceleration effect on the previous map would require

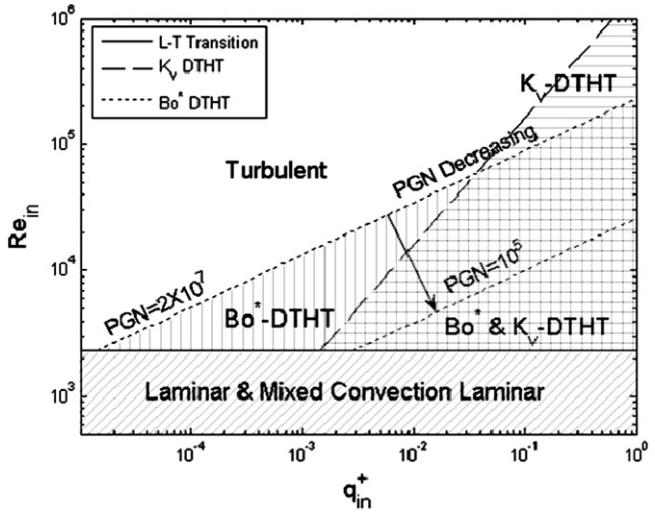

Fig. 9. Proposed heat transfer map.

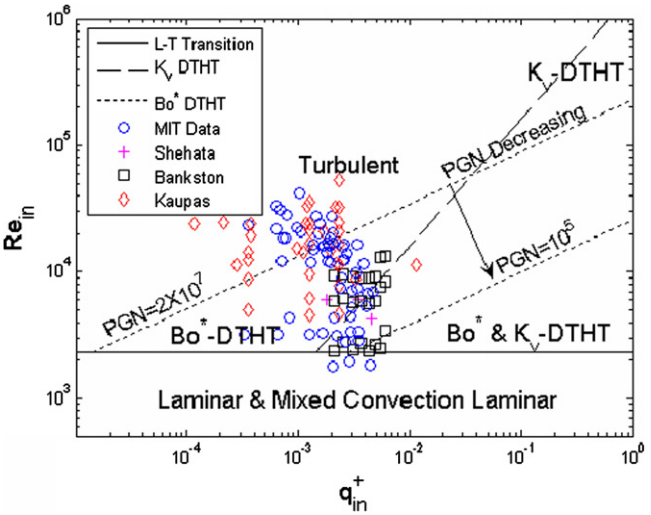

Fig. 10. MIT and other data from literature for the proposed regime map.

transformation of the Grashof number in a similar manner as the buoyancy parameter was transformed in the present study.

Secondly, the previous map demarcates the boundaries with the local Reynolds number and Grashof number while the new map evaluates the boundaries using the inlet Reynolds number and inlet non-dimensional heat flux evaluated with the fluid bulk temperature. The shift from the local parameters to the channel inlet parameters reflects the observation of experimental data trends. If one selects the inlet conditions for a regime determination, the boundary between the normal turbulent flow and DTHT regimes can be demarcated throughout the channel clearly (Fig. 8). Therefore, our experiments suggest that using inlet conditions as boundaries among different heat transfer regimes is a more appropriate approach than using non-dimensional numbers evaluated at local conditions, under uniform heat flux boundary condition and channel L/D below 110.[1] We expect this to hold for a broad range of gas flow heat transfer experiments since this reflects the nature of gas DTHT.

Lastly, the free convection regime for either laminar or turbulent flow from the previous map is missing in the proposed map. In a laminar flow case, the buoyancy effect does not induce abrupt change in the heat transfer coefficient compared to the DTHT regime. This result can be also observed in the work of others [17]. Thus, drawing a clear line between the laminar and the mixed-laminar regimes did not seem reasonable when comparing the characteristics of the DTHT boundaries to the laminar mixed convection boundary. A free convection turbulent boundary is not shown in the proposed map due to the lack of gas experimental data for that case. This lack is not surprising because pure free convection cannot be attained easily in a relatively small diameter tube, as used in this experimental facility (15.7 mm).

The limitations of the new heat transfer map are: (1) it shall be used only for gas flow, (2) it should be applied only for upward heated flow, (3) it is verified for the non-dimensional heat flux of this experimental dataset and (4) it applies to channels with uniform heat flux and L/D below 110.

Fig. 10 shows the experimental conditions of other literature sources along with the data presented in this paper. Even though there is a vast amount of experimental work related to the DTHT area with supercritical fluids and liquid water, only limited number of literature sources experimented with gas, and thus are selected for comparison, due to the uniqueness of gas thermo-physical properties change with temperature [10]. In the figure, "Shehata" indicates the experimental conditions from Ref. [18], "Bankston" data are from Ref. [19] and "Kaupas" are from Ref. [20]. It should be noted that the conditions shown in the figure are based on the inlet conditions. From the analysis of Ref. [21] with the data presented in Ref. [18], some "Shehata" data may have slightly experienced both the buoyancy DTHT and the acceleration DTHT and this possibility is demonstrated in the figure. "Shehata" data focused more on measuring the velocity and temperature profiles during the operation in the DTHT regime than obtaining the heat transfer coefficient, and three experiments were conducted with shorter L/D (~30) and larger diameter (27.4 mm) than the present experimental facility ($L/D \sim 110$, ID = 15.7 mm). "Bankston" data were obtained in the acceleration DTHT regime since he used a smaller diameter (~3 mm) and thereby reduced "PGN" to have negligible buoyancy effects on the turbulent flow. This is shown in the heat transfer map (Fig. 10) since a smaller "PGN" means smaller buoyancy driven DTHT regime leading a large portion of "Bankston" data to exist in the acceleration DTHT regime. In contrast, "Kaupas" data were obtained in the buoyancy driven DTHT since they used a relatively large diameter (36.3 mm) to increase "PGN" resulting in a larger effect of the buoyancy driven DTHT regime compared to "Bankston" data. "Shehata" and "Kaupas" obtained their data with air at atmospheric pressure, and "Bankston" utilized hydrogen and helium at atmospheric pressure.

4. Summary

Experimental heat transfer data for the gas up-flow in a circular heated channel with a near uniform heat flux were presented. Three gases were used in the experiment: nitrogen, helium, and carbon dioxide, which together with pressure variation made it possible to achieve a number of different heat transfer regimes. The experiments were particularly focused on two DTHT regimes: (1) buoyancy induced DTHT and (2) acceleration induced DTHT. The nitrogen data covered the acceleration driven DTHT and buoyancy driven DTHT, the helium data covered the mixed convection laminar, acceleration driven DTHT and laminar to turbulent transition regimes and the carbon dioxide data covered the re-turbulizing buoyancy driven DTHT and non-re-turbulizing buoyancy induced DTHT. The "re-turbulizing" buoyancy driven DTHT is a phenomenon in gas up-flow heat transfer identified by a change of the gas heat transfer regime back from the DTHT to the forced turbulent regime in the downstream section of a heated channel

[1] The value 110 is the maximum L/D for the present experimental facility.

due to a decrease in the buoyancy force along the channel. Both the acceleration driven DTHT and buoyancy driven DTHT showed reductions of up to 70% from the normal turbulent heat transfer. Thus, using a forced turbulent heat transfer correlation in the DTHT regime can underpredict the wall temperature substantially, e.g., 50% of the wall-to-bulk temperature difference. The validity of the data was established using an energy balance and uncertainty analysis. Using the new experimental data, we updated the traditional threshold (Ref. [6]) for the DTHT regime to account for phenomena observed and a new heat transfer regime map for the gas heated up-flow was proposed. This map was compared to other experimental data from literature sources and the map reasonably represents each experimental condition in the literature. The new data have been used to develop new heat transfer correlations, presented in an accompanying paper [7], to more accurately predict the DTHT regimes.

Acknowledgements

The authors would like to acknowledge financial support from the Idaho National Laboratory (INL) through the Strategic INL/MIT Nuclear Research Collaboration Program. They thank Dr. Glenn E. McCreery of INL for valuable comments on the design of the facility.

References

[1] P. Hejzlar, A modular, gas turbine fast reactor concept (MFGR-GT), Transactions of the American Nuclear Society, vol. 84, Milwaukee, Wisconsin, June 17–21, 2001.
[2] W.C. Williams, P. Hejzlar, M.J. Driscoll, Decay heat removal from GFR core by natural convection, in: International Congress on Advances in Nuclear Power Plants ICAPP'04, Paper 4166, Pittsburgh, USA, June 13–17, 2004.
[3] W.B. Hall, J.D. Jackson, Laminarization of a turbulent pipe flow by buoyancy forces, ASME 69-HT-55, 1969.
[4] W.M. Kays, M.E. Crawford, Convective Heat and Mass Transfer, third ed., McGraw-Hill, Inc., 1993.
[5] D.M. McEligot, C.W. Coon, H.C. Perkins, Relaminarization in tubes, Int. J. of Heat Mass Transfer 13 (1969) 431–433.
[6] D.M. McEligot, J.D. Jackson, Deterioration criteria for convective heat transfer in gas flow through non-circular ducts, Nucl. Eng. Des. (Short Commun.) 232 (2004) 327–333.
[7] J.I. Lee, P. Hejzlar, P. Saha, M.S. Kazimi, D.M. McEligot, Deteriorated heat transfer of gas up-flow in a circular tube: correlations, Int. J. Heat Mass Transfer, ibid.
[8] J.I. Lee, P. Saha, P. Hejzlar, M.S. Kazimi, Transitional flow from laminar to turbulent mixed convection in a heated vertical pipe, in: International Congress on Advances in Nuclear Power Plants (ICAPP'05), Paper 5320, Seoul, Korea, May 15–19, 2005.
[9] J.I. Lee, P. Saha, P. Hejzlar, M.S. Kazimi, Studies of the deteriorated turbulent heat transfer regime for the gas-cooled fast reactor decay heat removal system, in: International Conference on Nuclear Engineering (ICONE14)'06, Paper 89826, Miami, Florida, USA, July 17–20, 2006.
[10] J.I. Lee, P. Hejzlar, P. Saha, M.S. Kazimi, Studies of the deteriorated turbulent heat transfer regime for the gas-cooled fast reactor decay heat removal system, Nucl. Eng. and Des. 237 (2007) 1033–1045.
[11] P. Cochran, P. Saha, P. Hejzlar, D.M. McEligot, G.E. McCreery, R.R. Schultz, Scaling analysis and selection of test facility for fundamental thermal-hydraulic studies related to advanced gas-cooled reactor, INL/EXT-05-00158, Idaho National Laboratory and Massachusetts Institute of Technology, Department of Nuclear Science and Engineering, 2005.
[12] J.I. Lee, P. Hejzlar, P. Stahle, P. Saha, D.M. McEligot, G.E. McCreery, R.R. Schultz, Design of thermal-hydraulic loop related to advanced gas-cooled reactor, in: Third Annual Report, MIT-GFR-042, INL/EXT-06-11801, Idaho National Laboratory and Massachusetts Institute of Technology, Department of Nuclear Science and Engineering, September 2006.
[13] J.I. Lee, P. Hejzlar, M.S. Kazimi, Deteriorated turbulent heat transfer to up-flowing gas in a heated vertical channel, MIT-ANP-TR-115, Center for Advanced Nuclear Energy Systems, Massachusetts Institute of Technology, May 2007.
[14] V. Gnielinski, New equations for heat and mass transfer in turbulent pipe and channel flow, Int. Chem. Eng. 16 (2) (1976) 359–387.
[15] J.D. Jackson, M.A. Cotton, B.P. Axcell, Studies of mixed convection in vertical tubes, Int. J. Heat Fluid Flow 10 (1989) 2–15.
[16] B. Metais, E.R.G. Eckert, Forced, mixed and free convection regimes, J. Heat Transfer (1964) 295–297.
[17] T.M. Hallman, Experimental study of combined forced and free laminar convection in a vertical tube, NASA Technical Note, TN D-1104, December 1961.
[18] A.M. Shehata, D.M. McEligot, Mean structure in the viscous layer of strongly-heated internal gas flows. Measurements, Int. J. Heat Mass Transfer 41 (1998) 4297–4313.
[19] C.A. Bankston, The transition from turbulent to laminar gas flow in a heated pipe, Journal of Heat Transfer (1970) 569–579.
[20] V.E. Kaupas, P.S. Poškas, Effect of variability of the physical properties of the gas on combined (free and forced) convection heat transfer in vertical pipes, Scripta Technica, Inc., 1991.
[21] D.P. Mikielewicz, A.M. Shehata, J.D. Jackson, D.M. McEligot, Temperature velocity and mean turbulence structure in strongly heated internal gas flows. Comparison of numerical predictions with data, Int J. Heat and Mass Transfer 45 (2002) 4333–4352.